Carbon sources in the North Sea evaluated by means of radium and stable carbon isotope tracers

W. J. Burt,[*][1] **H. Thomas,**[1] **M. Hagens,**[2] **J. Pätsch,**[3] **N. M. Clargo,**[4] **L. A. Salt,**[5] **V. Winde,**[6] **M. E. Böttcher**[6]

[1]Department of Oceanography, Dalhousie University, Halifax, NS, Canada
[2]Department of Earth Sciences-Geochemistry, Utrecht University, Utrecht, Netherlands
[3]Department of Theoretical Oceanography, Institute of Oceanography, University of Hamburg, Hamburg, Germany
[4]Department of Marine Geology and Chemical Oceanography (GCO), Royal Netherlands Institute for Sea Research (NIOZ), Texel, Netherlands
[5]CNRS, UMR7144, Equipe Chimie Marine, Station Biologique de Roscoff, Place Georges Teissier, Roscoff cedex, France
[6]Geochemistry & Isotope Biogeochemistry Group, Marine Geology Department, Leibniz Institute for Baltic Sea Research (IOW), D-18119 Warnemünde, Germany

Abstract

A multitracer approach is applied to assess the impact of boundary fluxes (e.g., benthic input from sediments or lateral inputs from the coastline) on the acid-base buffering capacity, and overall biogeochemistry, of the North Sea. Analyses of both basin-wide observations in the North Sea and transects through tidal basins at the North-Frisian coastline, reveal that surface distributions of the $\delta^{13}C$ signature of dissolved inorganic carbon (DIC) are predominantly controlled by a balance between biological production and respiration. In particular, variability in metabolic DIC throughout stations in the well-mixed southern North Sea indicates the presence of an external carbon source, which is traced to the European continental coastline using naturally occurring radium isotopes (^{224}Ra and ^{228}Ra). ^{228}Ra is also shown to be a highly effective tracer of North Sea total alkalinity (AT) compared to the more conventional use of salinity. Coastal inputs of metabolic DIC and AT are calculated on a basin-wide scale, and ratios of these inputs suggest denitrification as a primary metabolic pathway for their formation. The AT input paralleling the metabolic DIC release prevents a significant decline in pH as compared to aerobic (i.e., unbuffered) release of metabolic DIC. Finally, long-term pH trends mimic those of riverine nitrate loading, highlighting the importance of coastal AT production via denitrification in regulating pH in the southern North Sea.

The ever-increasing threat of ocean acidification has been shown to be more severe in shallow continental shelf systems compared to the adjacent open ocean (Orr et al. 2005; Thomas et al. 2007; Wootton and Pfister 2012). This is due, in part, to the highly productive and shallow nature of many shelf regions, as well as their spatial and temporal complexities. The North Sea has been identified as a strong continental shelf pump system, where carbon dioxide (CO_2) invades into surface waters, and is exported below the thermocline into the deep ocean (Thomas et al. 2004). Coastal seas in densely populated regions also experience large fluxes of organic and inorganic nutrients from riverine, groundwater, and atmospheric nitrogen sources, further accelerating acidification (Doney et al. 2009; Borges and Gypens 2010; Lorkowski et al. 2012; Duarte et al. 2013). The susceptibility of such regions has led to numerous studies focused on

describing the North Sea carbonate system (Bozec et al. 2005; Bozec et al. 2006; Thomas et al. 2009), and its change over time (Salt et al. 2013; Clargo et al. 2015).

By separating out the inputs of carbon from the North Atlantic Ocean (via the Faire Island, Shetland, and English Channels), Thomas et al. (2005) developed a net carbon budget of the North Sea which was dominated by three major inputs: European continental rivers, the atmosphere, and import from the Baltic Sea. Before reaching the open North Sea, many of these rivers empty into the shallow intertidal areas of the Wadden Sea, a region known to play an important role in the biogeochemical cycling of the North Sea (Brasse et al. 1999; Thomas et al. 2009; Omar et al. 2010; Winde et al. 2014a; Santos et al. 2015). Schwichtenberg et al. (2012) concluded that annual changes in total alkalinity (AT) for the southeastern North Sea (the German Bight) are controlled predominantly by inputs from the Wadden Sea. Intense primary production, along with water column and benthic remineralization of organic matter, also

*Correspondence: willburt86@gmail.com

alters the North Sea carbonate system throughout the year. Whereas it is clear that various important carbon fluxes exist in the North Sea, it remains difficult to resolve how each source or process contributes to the carbon content of the North Sea at any given location (Pätsch and Kühn 2008; Kühn et al. 2010).

The stable carbon isotope composition of dissolved inorganic carbon ($\delta^{13}C_{DIC}$) is of particular value for distinguishing and tracing sources, sinks and transformations of carbon in the water column (Quay and Stutsman 2003) and for identifying benthic-pelagic coupling (Boehme et al. 1996; Fry 2002; Hu and Burdige 2007; Dorsett et al. 2011). In the open ocean, spatial variability of $\delta^{13}C_{DIC}$ is typically quite small, and is considered to reflect a balance between biological and thermodynamic processes (Gruber et al. 1999). Air–sea exchange, and its temperature dependence, can also play an important role in altering $\delta^{13}C_{DIC}$ in large ocean basins, where residence times of surface waters far exceed those required for isotopic equilibrium between the atmosphere and surface ocean (~ 10 yr). Indeed, changes in $\delta^{13}C_{DIC}$ due to the continual input of isotopically light anthropogenic CO_2 into the world's oceans (known as the oceanic so-called "Suess" effect), have been used to estimate accumulation rates of anthropogenic carbon in ocean waters (Quay et al. 2007), as well as to elaborate on paleoclimate scenarios (Olsen and Ninnemann 2010). Overall, the dominant controls on $\delta^{13}C_{DIC}$ signals are thought to be well known for open ocean systems (Gruber et al. 1999; Racapé et al. 2013). In coastal systems, spatial and temporal variabilities of $\delta^{13}C_{DIC}$ are often much more pronounced, and freshwater sources further confound the signal. As a result, much less is known regarding the dominant controls governing the $\delta^{13}C_{DIC}$ distributions in a given coastal region. The substantial difference in the carbon isotope composition of DIC in different water masses, however, offers a high potential for the use of $\delta^{13}C_{DIC}$ to separate sources and sinks in complex near-coastal carbonate systems. In tidal areas of the southern North Sea, for instance, Winde et al. (2014a,b,c) used covariations in $\delta^{13}C_{DIC}$ and DIC to identify key inputs from different freshwater sources (submarine groundwater discharge, rivers, and small inlets) and North Sea waters, and demonstrated that mixing between these water masses substantially affects the $\delta^{13}C_{DIC}$, DIC, and pCO_2 observed in the shallow water column of the Wadden Sea.

The Wadden Sea is also a source of two naturally occurring radium isotopes, ^{224}Ra and ^{228}Ra, to the North Sea (Moore et al. 2011). These two isotopes, along with ^{223}Ra and ^{226}Ra, make up the radium isotope quartet, a group of tracers that have become widely used tools to investigate the extent and impact of land-derived inputs to coastal waters (Charette and Scholten 2008). Both ^{224}Ra and ^{228}Ra have thorium (Th) parent isotopes that are strongly adsorbed to particle surfaces, thus both will enter the water column at two major sediment-water column boundaries, the seafloor and the coastline. Due to their vastly differing half-lives ($t_{1/2}$), these isotopes are indicators of very different processes. On basin-wide scales, short-lived ^{224}Ra ($t_{1/2} = 3.7$ d) has a negligible coastal signal as it cannot disperse far offshore before decaying, but it has a strong benthic signal because it can rapidly regenerate in sediment pore waters. As a result, ^{224}Ra is considered to be a direct tracer of sediment-water column interaction in the shallow well-mixed waters of the southern North Sea (Burt et al. 2014). In contrast, longer-lived ^{228}Ra ($t_{1/2} = 5.8$ yr) can be transported vast distances away from its source regions, but regenerates very slowly in sediments (Moore 2007). Consequently, coastal ^{228}Ra fluxes, which include inputs from rivers and submarine groundwater discharge, are often 1–2 orders of magnitude larger than fluxes from the seafloor (Moore 2007; Moore et al. 2011). Therefore, ^{228}Ra can be utilized to trace the dispersion of dissolved materials away from a coastal source, such as the Wadden Sea.

In this study, a novel multitracer approach is utilized to quantify inputs and transformations of carbon in the North Sea that play an important role in regulating present and future rates of coastal acidification in the region. First, the dominant controls on the AT, DIC and $\delta^{13}C_{DIC}$ distributions of surface waters are discussed. Relationships between DIC, $\delta^{13}C_{DIC}$, and Ra are then used to quantify a coastal carbon source in the North Sea. A strong relationship is found between AT and ^{228}Ra, which supports the use of ^{228}Ra as an AT tracer. Coastal inputs of ^{228}Ra, metabolic DIC and metabolic AT are then derived on basin-wide scales and ratios of coastal DIC and AT inputs are used to infer the dominant processes responsible for their formation. Finally, the extent to which these coastal AT inputs affect the buffering capacity of the southern North Sea is assessed.

Oceanographic setting

The major water masses of the North Sea, as well as a generalized circulation pattern, are shown in Fig. 1. The largest input is from the North Atlantic, which enters primarily through the Shetland and Faire Island Channels at the northern boundary and circulates counter-clockwise before exiting through the deep Norwegian trench. Much of this circulation is limited to the north and central North Sea, with as little as 5% of this North Atlantic water flowing through the southern region (Turrell et al. 1992; Lenhart and Pohlmann 1997).

A small fraction of North Atlantic water also enters via the English Channel, and flows into the southern North Sea. European continental runoff enters the North Sea via various rivers and groundwater sources along the European continental coast, and predominantly flows northeast along the coast as continental coastal water. A large fraction of this runoff is transported to the North Sea via exchange with the Wadden Sea, a shallow tidal mudflat region that extends across much of the continental coastline (*see* Fig. 1). English Channel water and European continental runoff are the main components of the Southern or German Bight water
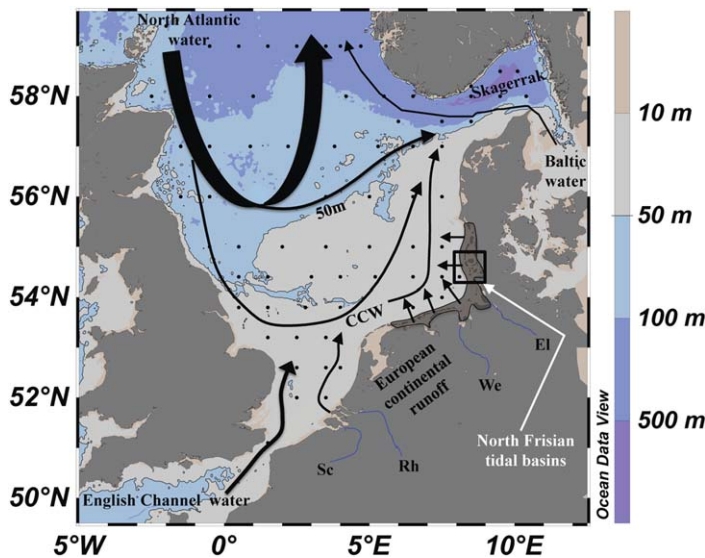
Fig. 1. Map of North Sea with stations sampled during 2011 cruise (black dots). The 50 m contour roughly traces the border between well-mixed stations to the south, and stratified stations to the north. The Wadden Sea is outlined in the black shaded area and the location of the North Frisian tidal basins is shown. Black arrows show the general circulation pattern and the inputs of primary water masses (from Turrell et al. 1992). Widths of the arrows roughly illustrate the magnitude of volume transport. CCW = Continental coastal waters, and major rivers are labeled: Sc = Scheldt, Rh = Rhine, We = Weser, El = Elbe.

mass. Baltic Sea water enters the North Sea via the Skagerrak and exits via the Norwegian Trench (Lee 1980).

Methods

Sample collection and analysis

North Sea water column samples were collected during a basin-wide North Sea survey conducted in September 2011, aboard the *R/V Pelagia* (as part of the NWO, Netherlands Organization for Scientific Research National Programme Sea and Coastal Research ZKO grant number 839.10.500). Conductivity, temperature, and pressure, along with rosette bottle sampling for DIC, AT, and $\delta^{13}C_{DIC}$ were conducted in vertical profiles at 88 stations. DIC and AT were analyzed onboard using a dual VINDTA 3C system provided by the Royal Netherlands Institute for Sea Research (NIOZ). Further detail regarding collection, analysis, and interpretation of DIC and AT from the 2011 cruise is given by Clargo et al. (2015), and details of the respective coulometric and potentiometric determinations for DIC and AT are provided by Thomas et al. (2007). $\delta^{13}C_{DIC}$ samples were collected in 30 mL glass serum bottles and 60 μL of a HgCl$_2$ solution were injected to halt biological activity. Surface water samples on the three North Frisian transects were collected within the German BIOACID program in September 2009, aboard *R/V Mya*. Samples for AT and $\delta^{13}C_{DIC}$ were collected in 12 mL Exetainers® prefilled with 100 μL of a HgCl$_2$ solution. Temperature was measured on-board and salinity was calculated from conductivity measurements carried out with a Condi1970i meter equipped with a TetraCon325 cell. The analytical procedures are further described in Winde et al. (2014a).

Analysis of $\delta^{13}C_{DIC}$ was carried out by means of continuous-flow isotope-ratio-monitoring mass spectrometry (CF-irmMS) on Thermo Finnigan MAT 253 gas mass spectrometers coupled to a Thermo Electron Gas Bench II via a Thermo Electron Conflo IV split interface at Utrecht University and Leibniz IOW. The North Sea water column samples were analyzed at Utrecht University, using Li$_2$CO$_3$ (LSVEC) and Na$_2$CO$_3$ solutions for calibration. The samples from the tidal basins were analyzed at Leibniz IOW using NBS-19, LSVEC, a carbonate from Solnhofen (Germany), and NaHCO$_3$ solutions for calibration. Stable carbon isotope ratios are expressed in the usual δ-notation as per mil (‰) deviation relative to the international Vienna Pee Dee Belemnite (VPDB) standard. The analytical method in both laboratories has a reproducibility of better than ± 0.1‰.

Ra isotopes were collected onto MnO$_2$-coated acrylic fibers from surface waters (5 m) at 61 stations, with near-bottom vertical profiles conducted at 13 stations. ^{224}Ra activities were determined using the Radium Delayed Continuous Counting system (RaDeCC) system. All samples were counted within 2 d of sample collection to avoid significant ^{224}Ra decay. Samples were then recounted between 7 d and 13 d after collection to determine activities of supported ^{228}Th, which were subtracted to obtain excess ^{224}Ra activities. Although some ^{224}Ra remains on the fiber during the second count, it can be assumed that only the unsupported ^{224}Ra decays during the days between counts, and thus the supported component of ^{224}Ra (i.e., the ^{228}Th activity) can be calculated using the following equation (M. Rutgers van der Loeff pers. comm.):

$$\frac{^{228}\text{Th} = {}^{224}\text{Ra}_{t1} - {}^{224}\text{Ra}_{t2}e^{\lambda dt}}{1 - e^{\lambda dt}} \tag{1}$$

Where ^{224}Ra$_{t1}$ and ^{224}Ra$_{t2}$ refer to supported radium activities obtained from the first and second counts respectively, λ is the ^{224}Ra decay constant (0.189 per day), and dt is the time interval in days between the first and second counts. More detailed methods for Ra isotope collection and analysis of ^{224}Ra are described by Burt et al. (2014). ^{224}Ra uncertainties range from 7% to 23%.

Following ^{224}Ra analysis, fibers were allowed to age for > 36 months before recounting on the RaDeCC. After this aging time, a significant amount of the original ^{228}Ra will have decayed to ^{228}Th. Having calculated the original ^{228}Th attached to the fiber using the equation above, the counts recorded from the aged fiber can yield the extent of ^{228}Th ingrowth, which, using the various decay constants, can be used to back calculate the activity of ^{228}Ra at the time of sampling. Uncertainties for both ^{224}Ra and ^{228}Ra activities are calculated using the propagation of error technique described by Garcia-Solsona et al. (2008). Uncertainties for individual ^{228}Ra counts range from 5% to 8%. For samples counted multiple

times ($n = 27$), the resulting activities and uncertainties are averaged. Samples counted multiple times show good agreement between their individual measurements, with a mean relative standard deviation of 6% for the 27 samples.

Determination of the biological component of DIC (DIC_{bio})

The surface water DIC concentration of a given water mass is altered by air–sea gas exchange, the biological production/consumption of organic matter, and calcium carbonate ($CaCO_3$) formation/dissolution. Therefore, to isolate the biological component, a surface DIC concentration at atmospheric equilibrium is computed and subsequently removed from the observed DIC (DIC_{obs}):

$$DIC_{bio} = DIC_{obs} - DIC_{pCO2=383.26} \qquad (2)$$

At each station, $DIC_{pCO2=383.26}$ is computed using the same in situ temperature, salinity, and alkalinity as the corresponding DIC_{obs}. The atmospheric equilibrium value of 383.26 μatm is the average atmospheric pCO_2 in September 2011, as measured at the Mace Head atmospheric station in Ireland (53.326°N, 9.899°W) as obtained from the National Oceanic and Atmospheric Administration Climate Monitoring and Diagnostics Laboratory air sampling network (http://www.cmdl.noaa.gov/). This calculation (Eq. 2) has been used previously to determine excess DIC in subsurface waters to assess the potential extent of CO_2 outgassing during coastal upwelling (Borges 2011; Burt et al. 2013).

The DIC_{bio} calculation assumes that any excess or deficit from the atmosphere-equilibrated DIC value ($DIC_{pCO2=383.26}$) is due solely to biological processes. However, compared to oxygen, atmospheric equilibration of CO_2 is relatively slow, and thus deviations in $DIC_{pCO2=383.26}$ could be related to other processes that occur on relatively short time scales (i.e., a few weeks). Air–sea exchange of CO_2 over short (e.g., weekly) timescales has a negligible effect on DIC concentrations. Physical processes, notably a change in water temperature, could alter the pCO_2 of surface waters relatively rapidly (i.e., before CO_2 air–sea equilibration occurs), and thus, alter the $DIC_{pCO2=383.26}$ term. Therefore, this method also assumes that surface water temperature does not vary, or varies only incrementally in the weeks preceding the observations. Sea surface temperatures throughout the North Sea are relatively stable during the summer plateau, with slight declines beginning in September (Prowe et al. 2009). According to the A12 CPP weather station in the central North Sea (55.399°N, 3.810°E), daily maximum air temperatures in August 2011 and September, 2011 averaged 15.6°C and 15.3°C, respectively (http://www.ncdc.noaa.gov/). If sea surface temperatures cooled by the same amount (i.e., 0.3°C), $DIC_{pCO2=383.26}$ would be overestimated by ~2–3 μmol/kg, resulting in underestimation of the same magnitude of the respiratory (i.e., positive) component of DIC_{bio}. Changes of this magnitude are insignificant compared to the range of values observed in this study. Furthermore, since short term temperature changes will be comparable throughout the North Sea, their impact on the spatial variability of DIC_{bio} can be deemed minor.

Finally, an assumption must be made regarding the formation and dissolution of $CaCO_3$, as this process will also alter DIC_{bio}. In general, calcification is not considered a significant component of the carbon cycle compared to processes such as organic matter production/respiration, air–sea exchange, and water-mass mixing (Bozec et al. 2006). In the southern North Sea, the upper limit for benthic carbonate dissolution has been estimated at 2.7 mmol C/m^2 per day (Brenner et al. 2015; F. Gazeau pers. comm.). Comparatively, benthic remineralization rates measured in the southern North Sea during the 2011 cruise ranged from 3.1-28.7 mmol C/m^2 per day, and pelagic remineralization was estimated at 36.5 mmol C/m^2 per day (Brenner et al. 2015). With this in mind, we consider the effects of $CaCO_3$ formation/dissolution on DIC_{bio} to be relatively minor compared to the effect of organic matter production/respiration.

Given these assumptions, an increase in DIC_{bio} represents the production of DIC via the respiration of organic matter, whereas a decrease represents the uptake of DIC by primary producers during photosynthesis. As this statement implies, DIC_{bio} is used as a relative property, meaning that only relative changes in its magnitude are considered, rather than the magnitude of any particular value itself.

Results and discussion

North Sea surface distributions

The surface distributions of $\delta^{13}C_{DIC}$, Ra isotopes, AT, and salinity in the North Sea show well-defined areas of low and high concentrations (Fig. 2). First, in the three top panels of Fig. 2, an abrupt change in $\delta^{13}C_{DIC}$ (a) and ^{224}Ra (b) distributions occurs at the border between stratified waters to the north, and fully mixed waters to the south (stratification conditions shown in panel c). The effect of stratification on the vertical structure of $\delta^{13}C_{DIC}$ in the water column is shown in Fig. 3. In the deeper northern North Sea, much of the organic matter formed in surface waters sinks and is respired below the pycnocline. This creates a spatial separation of production and respiration, with surface waters exhibiting the enriched $\delta^{13}C_{DIC}$ signal indicative of net production, and $\delta^{13}C_{DIC}$ depletion in deeper waters due to net respiration (Fig. 3). In contrast, organic matter produced within the fully mixed southern North Sea cannot escape to any subsurface layer and is thus respired in the mixed water column, or via recycling through the underlying sediments. The result is a net balance between production and respiration in the southern North Sea, exemplified by a vertically homogeneous $\delta^{13}C_{DIC}$ signature which is relatively depleted compared to surface waters further north, and relatively enriched compared to deeper waters further north (Figs. 2, 3).

With regards to ^{224}Ra, surface waters in the stratified northern region are highly depleted because the majority of
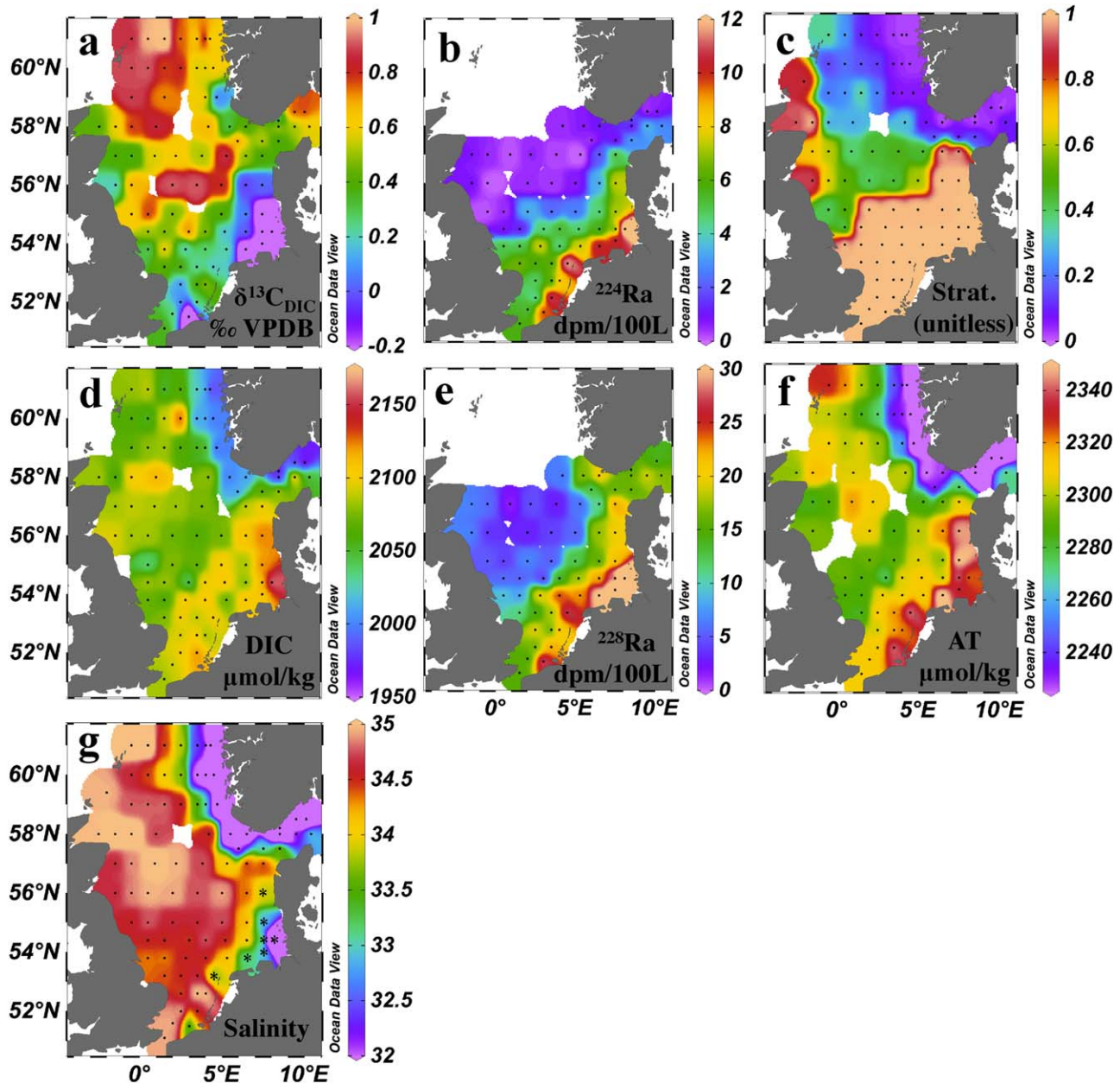
Fig. 2. Surface maps of various properties. "Strat." refers to stratification factor (mixed layer depth/bottom depth), where 1 represents a fully mixed water column. Stations labeled as low salinity ($S < 34$) throughout the manuscript are marked by asterisks (*, in panel g). Both AT and DIC were not available at the low-salinity station near the Scheldt/Rhine rivers (51.5°N, 3.0°E), thus are not included in further analyses, and the station is not labeled with an asterisk. Note that the strong minimum values of $\delta^{13}C_{DIC}$ and salinity ($\delta^{13}C_{DIC} = -1.92‰$, $S = 29.3$), as well as the maximum Ra activities ($^{224}Ra = 14.4$ dpm/100 L, $^{228}Ra = 47.4$ dpm/100 L) in the Elbe Estuary are not well represented by the scales. The DIC data have also been displayed by Clargo et al. (2015).

the ^{224}Ra signal generated by seafloor sediments decays within the deeper layer. In the fully mixed southern North Sea, sediments are in direct contact with surface waters, resulting in high surface water ^{224}Ra activities throughout the region (Fig. 2, panel b). This relationship between stratification conditions and surface ^{224}Ra activity is also shown using vertical profiles of ^{224}Ra and density at various North Sea stations (*see* Burt et al. 2014).

Surface distributions (Fig. 2) display a distinct source of DIC, AT, Ra, and freshwater from the European continental coastline. The highest AT values are located near the northern Wadden Sea, along the Danish (Jutland) and North Frisian coastline, in agreement with results from Schwichtenberg (2013), who found that this region of the Wadden Sea produces more AT than the southern region. Surface salinity (Fig. 2, panel g) reveals the major freshwater
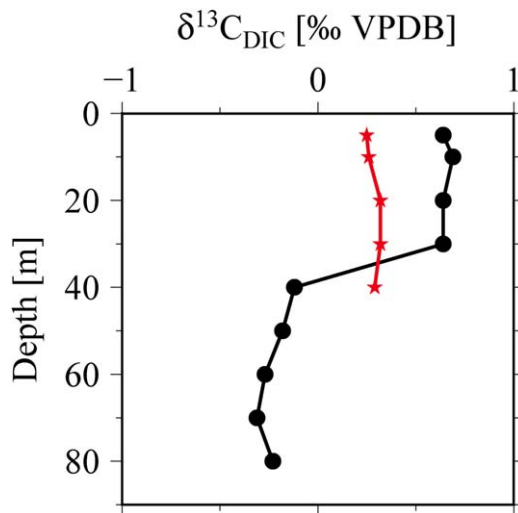
Fig. 3. $\delta^{13}C_{DIC}$ vertical profiles in the southern mixed region (red stars, station 16, 53.8°N, 4.0°E) and in the northern stratified region (black circles, station 47, 57.0°N, 2.2°E)

inputs to the North Sea, most notably the Baltic Sea (via the Skagerrak), and the major European rivers. Aside from the Scheldt and Rhine Rivers, which empty into the southern North Sea near the southernmost station (51.5°N, 3.0°E), these rivers empty first into the Wadden Sea and then into the German Bight. Outside of the Skagerrak, the salinity minimum is located in the southeastern corner of the sampling grid (54.4°N, 8.1°E) at the mouth of the Elbe River estuary. Here, a minimum $\delta^{13}C_{DIC}$ value and maximum Ra activities are also observed. Prior studies have shown that for ^{224}Ra, this coastal source does not extend beyond stations that border the European continental coastline before decaying completely (Schmidt et al. 2011; Burt et al. 2014).

The influence of the Wadden Sea coastline on surface distributions is examined further in Fig. 4. First, markedly high AT (> 2700 μmol/kg) and depleted $\delta^{13}C_{DIC}$ are observed in the Eider River, displaying the importance of riverine input at this particular drainage basin in contributing AT and a depleted $\delta^{13}C_{DIC}$ signal to North Sea coastal waters. A scatter plot of salinity and $\delta^{13}C_{DIC}$ throughout the North Sea stations (Fig. 4d) highlights this freshwater signal. In contrast, salinity remains relatively constant throughout the Hörnumtief and Nordenaue transects, yet significant changes in AT and $\delta^{13}C_{DIC}$ occur along both, with higher AT and more depleted $\delta^{13}C_{DIC}$ at the shoreward stations. This points instead to metabolic processes that occur while waters are flushed through the tidal basins. Local freshwater and metabolic AT sources, either individually or in combination, may explain the higher AT observed in the northern Wadden Sea compared to the southern region. Indeed, Fig. 4d,e highlight the importance of freshwater input (salinity dependent) and biological processes (salinity independent) in controlling distributions of AT and $\delta^{13}C_{DIC}$ at both a small scale within tidal basins and at a

larger scale throughout the entire North Sea. This biological (or metabolic) control on the $\delta^{13}C_{DIC}$, DIC, and AT distributions of the open North Sea will be described in detail throughout the remainder of the discussion. In summary, Figs. 2–4 illustrate the importance of the stratification pattern in governing the $\delta^{13}C_{DIC}$ and ^{224}Ra distributions, as well as the role of the continental coastline in supplying Ra, AT, and isotopically light carbon to the North Sea.

Processes affecting DIC and its isotopic signature ($\delta^{13}C_{DIC}$)

The processes that may cause variations in the concentration and stable isotope composition of DIC are: photosynthesis and respiration of organic material (termed together as biological or metabolic processes), invasion and degassing of CO_2 (termed together as air–sea exchange), $CaCO_3$ dissolution and formation, and addition of freshwater (e.g., Winde et al. 2014a). These processes and their impacts in coastal systems are illustrated in a DIC vs. $\delta^{13}C_{DIC}$ plot as introduced by Winde et al. (2014a,b,c). These authors describe the processes that may be important in coastal waters like the Wadden Sea. Following this approach, the estimates for the slopes in a DIC vs. $\delta^{13}C_{DIC}$ plot for each process of relevance for the open North Sea are given in Fig. 5. Observed results are then compared to these estimated slopes to evaluate the dominant process governing DIC and $\delta^{13}C_{DIC}$.

Surface water $\delta^{13}C_{DIC}$ distributions show substantial variability within the North Sea, ranging from −1.92‰ to 1.04‰ VPDB (Fig. 5a). The magnitude of this variability is due in large part to the addition of freshwater at the European coastline, as seen in Figs. 2 (panels a and g), and 4. Rivers and groundwater are often depleted in $\delta^{13}C_{DIC}$, due to dissolution of biogenic carbon ($\delta^{13}C_{DIC} \sim -25$‰) in soils (Spiker 1980) often superimposed by interactions with carbonate aquifer rocks (Deines et al. 1974; Böttcher 1999). Considering only the basin-wide North Sea samples collected in 2011, a best-fit line drawn through data from the lower salinity stations near the Wadden Sea (Fig. 4d, inset) yields a zero-salinity endmember of −15.0 ± 0.8‰. An inclusion of the 2009 data from the tidal basins within the Wadden Sea (Fig. 4d) provides a larger salinity range and yields an endmember of −12.8 ± 0.2‰. Both of these values are consistent with typical freshwater endmembers (Ahad et al. 2008), including those reported for small tributaries entering the Wadden Sea (−15‰ to −16‰, Winde et al. 2014a), and the Elbe River, the major freshwater source to the German Bight (about −12‰, Amann et al. 2015; Böttcher unpubl.). The DIC concentrations in European rivers also vary considerably, ranging from approximately 2195 μmol/kg in the Elbe River (Pätsch and Lenhart 2011), to more than 3000 μmol/kg DIC in some smaller tributaries (Winde et al. 2014a). Using an estimate for the Elbe River as an endmember ($\delta^{13}C_{DIC} = -12$‰ and DIC = 2195 μmol/kg) along with average values calculated from the open North Sea in 2011 ($\delta^{13}C_{DIC} = 0.39$‰ and DIC = 2088 μmol/kg), a two-point mixing
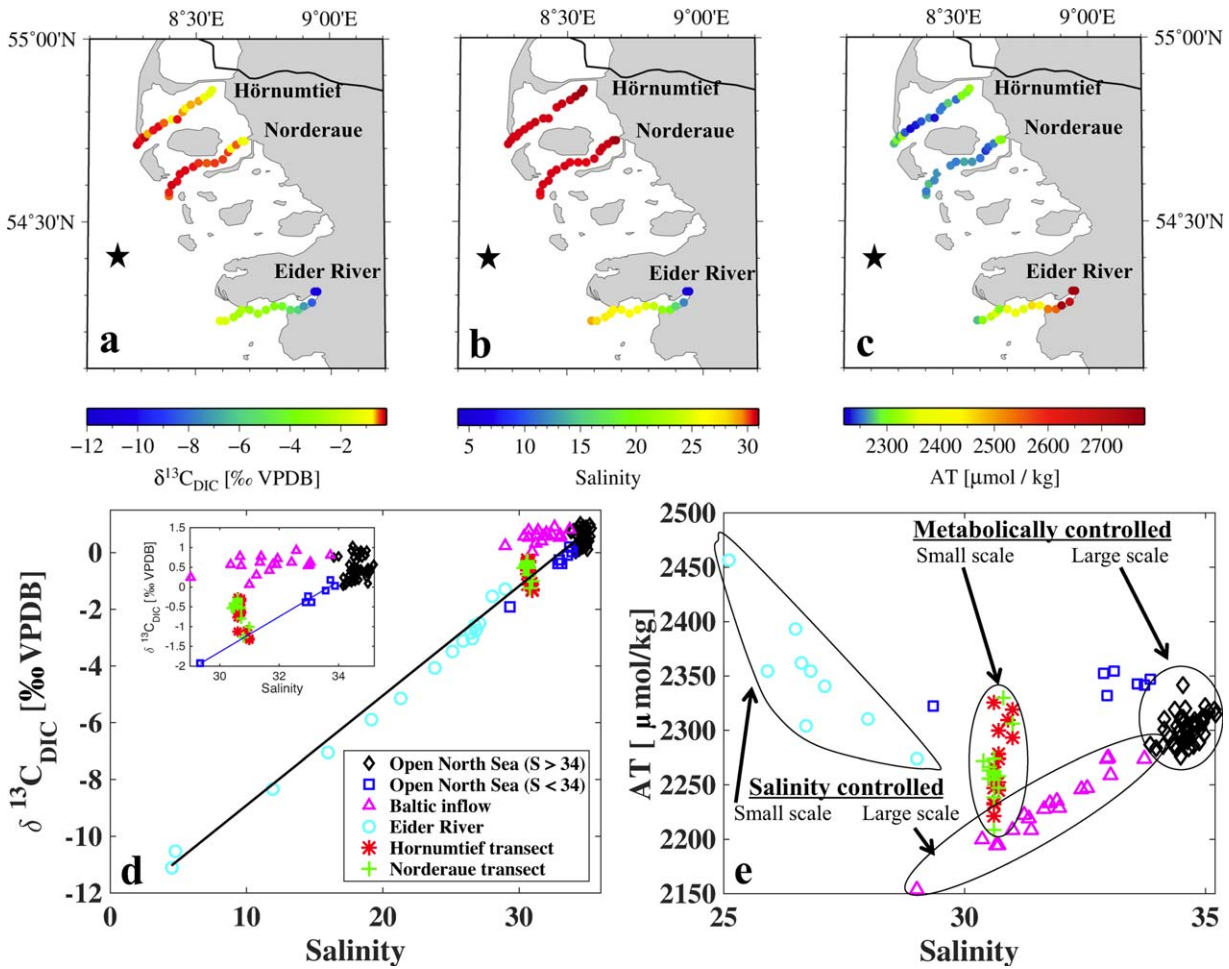
Fig. 4. Surface maps of $\delta^{13}C_{DIC}$ **(a)**, salinity **(b)**, and alkalinity **(c)** along 3 transects in North Frisian tidal basins. The black star indicates the Elbe Estuary station in the southeast corner of the North Sea sampling grid (*see* Fig. 1). **d**: Salinity relationship with $\delta^{13}C_{DIC}$. Regression is placed through all data excluding the Baltic inflow. Inner panel shows data at the high salinity band, with regression placed through low salinity stations near the coast (labeled with * in Fig. 2). **e**: Relationships between alkalinity and salinity for all stations. Inputs of freshwater and biological activity are shown to play an important role in altering alkalinity both at small scales within tidal basins, and throughout the entire North Sea. It is important to note that while both the North Frisian transects and North Sea data were collected in September, the former were collected in 2009, while the latter are from 2011.

line with a slope of -0.1 (‰ per μmol/kg) is calculated. This slope is considered a lower (i.e., most negative) limit, as smaller tributaries with much higher DIC concentrations will yield considerably shallower slopes (i.e., slopes closer to zero).

Marine primary producers preferentially take up light carbon when assimilating the DIC from seawater into organic carbon during photosynthesis. The extent of this preferential uptake is quantified using the biological fractionation factor, which can be approximated by the difference of the delta (δ) values between the reactant compound (in this case, DIC in seawater) and the product compound (i.e., organic carbon) (Zeebe and Wolf-Gladrow 2001). In contrast, respiration of organic material releases this isotopically light carbon back into the water column. Given these coupled reactions, Broecker and Maier-Reimer (1992) surmised that, when considering only bio-

logical processes, $\delta^{13}C_{DIC}$ should be tightly correlated to dissolved phosphate concentrations, and that a plot of these two variables should produce a slope (x) according to the equation:

$$x = \frac{\varepsilon}{DIC_{avg}} * \left[\frac{C}{P} \right]_{OM} \tag{3}$$

where DIC_{avg} is the average DIC concentration, ε is the biological fractionation factor, and the final term is the carbon to phosphate (C/P) ratio of organic matter. Here, we assume that dividing x by the C/P ratio yields a slope that corresponds solely to biological processes on a plot of $\delta^{13}C_{DIC}$ against DIC. According to Zeebe and Wolf-Gladrow (2001) and Hoefs (2015), biological fractionation factors in marine plankton vary between $-18‰$ and $-32‰$. Accordingly, we use a mid-range value of $-25‰$ and divide by the average
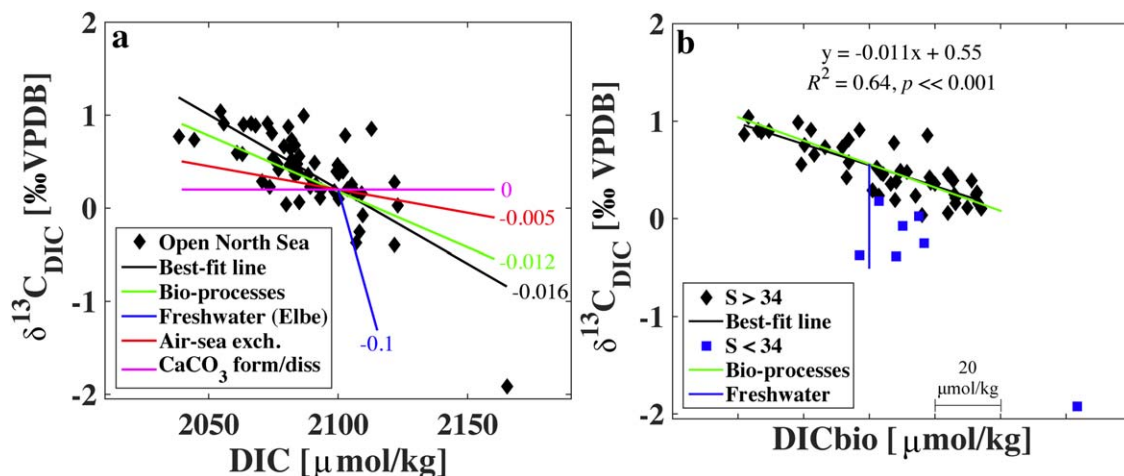
Fig. 5. a: Relationships between DIC and $\delta^{13}C_{DIC}$. The colored lines (with accompanying slopes) represent the estimated effects of biological uptake and respiration (bioprocesses), air–sea exchange (exch.), carbonate formation/dissolution (CaCO$_3$ form/diss), and freshwater input from the Elbe river, on the correlation. The least-squares regression and its corresponding slope are shown for comparison (black line). **b**: Covariations of DIC$_{bio}$ and $\delta^{13}C_{DIC}$. Note that the least squares regression line (black line, statistics are shown) does not include lower salinity stations ($S < 34$), which fall below the general trend in the data. DIC$_{bio}$ is a relative variable, thus no absolute values are shown along the x-axis, but each tick mark represents a DIC$_{bio}$ change of 20 μmol/kg. Stations within the Skagerrak region are not shown.

DIC (2088 μmol/kg, *see* above) to obtain a slope of -0.012. If respiration of organic material occurs via anaerobic processes, the produced anoxic pore water can carry a depleted $\delta^{13}C_{DIC}$ signal due to the addition of CO$_2$ from the mineralized organic matter (of about -20‰) superimposed by the possible formation and oxidation of methane (with $\delta^{13}C_{CH4}$ in shallow sediments of the southern North Sea of about -70‰) (Böttcher et al. 2007), considering that reactions involving methane may lead to a wide range in DIC isotope signatures (Heuer et al. 2009; Meister et al. unpubl.). Given that pore waters are often enriched in isotopically light DIC, their addition will affect the covariation of DIC and $\delta^{13}C_{DIC}$ in a matter similar to aerobic respiration (Winde 2013; Winde et al. 2014a). Therefore, the slope attributed to "biological processes" includes both aerobic and anaerobic respiration processes, despite the fact that a quantitative understanding of how anoxic pore water addition contributes to the estimated slope of -0.012 is not known at present.

CO$_2$ invasion increases DIC but decreases $\delta^{13}C_{DIC}$ because atmospheric CO$_2$ is isotopically light (approximately -7.8‰ in 1995 and decreasing by ~ 0.024‰ per year; Francey et al. 1999; Olsen et al. 2006). During CO$_2$ outgassing the lighter ^{12}C isotope is favored, causing $\delta^{13}C_{DIC}$ of surface waters to increase slightly while DIC decreases (Inoue and Sugimura 1985; Michaelis et al. 1985). Inoue and Sugimura (1985) list fractionation factors of -10‰ and -8‰ for CO$_2$ invasion and outgassing, respectively, and according to Lynch-Stieglitz et al (1995), a 1 μmol/kg increase in DIC due to CO$_2$ invasion induces a 0.005‰ decrease in $\delta^{13}C_{DIC}$. With this in mind, and given the first-order nature of this exercise, outgassing and invasion are assigned opposing slopes of the

same magnitude ($+0.005$ and -0.005, respectively, *see* Fig. 5a). Isotopic fractionation during CaCO$_3$ formation is only small (less than $+2$‰; Michaelis et al. 1985) and CaCO$_3$ dissolution involves no fractionation, but the impact on DIC will depend on the isotopic composition of the dissolving solid (Deines et al. 1974; Böttcher 1999). For simplicity, it is assumed here that CaCO$_3$ formation and dissolution only affect DIC concentrations, and thus have a slope of zero.

The observed covariation between DIC and $\delta^{13}C_{DIC}$ from the 2011 North Sea cruise is shown in Fig. 5a. A linear least-squares regression of these data yields a best-fit line with a slope of -0.016. This slope compares well to that of biological processes (-0.012), suggesting the importance of photosynthesis and respiration in governing the covariation in the open North Sea. This is similar to the relationship reported by Winde et al. (2014a,b). However, this analysis cannot rule out the possibility of two or more processes biasing the slope in opposing directions (freshwater input and CO$_2$ uptake, for example). Without further information regarding specific freshwater sources or rates of either air–sea exchange or carbonate formation/dissolution from the 2011 cruise, distinguishing between these two interpretations is difficult. To investigate this further, we simplify the diagram in Fig. 5a by introducing DIC$_{bio}$, which isolates biological changes in DIC.

The DIC$_{bio}$ term assumes that, prior to being affected by biological processes, all waters are equilibrated with the atmosphere, in accordance with the in situ temperature and salinity, and removes this equilibrated DIC from the observed value. As illustrated by the shallow-slope in Fig. 5a, the effects of air–sea exchange are much smaller for $\delta^{13}C_{DIC}$

than for DIC, because chemical equilibrium of CO_2 between the ocean and atmosphere occurs approximately 10 times more rapidly than isotopic equilibrium (Gruber et al. 1999). In coastal systems like the North Sea, where the residence time of waters is relatively short compared to that of the open ocean, changes in $\delta^{13}C_{DIC}$ due to isotopic equilibration will be even smaller, and thus, in this study are not considered to be important. Therefore, air–sea interaction is considered to have no effect on the covariation between DIC_{bio} and $\delta^{13}C_{DIC}$.

The covariation of $\delta^{13}C_{DIC}$ with DIC_{bio} is shown in Fig. 5b. Freshwater addition, regardless of its source, is now illustrated with a single vertical slope, as DIC_{bio} takes into account any salinity-dependent changes in DIC. When excluding stations with discernible freshwater input (salinities < 34), a strong correlation exists between DIC_{bio} and $\delta^{13}C_{DIC}$ (Fig. 5b), which we assume is related exclusively to biological processes.

The slope of the linear regression (−0.011) is nearly identical to the theoretical slope for biological processes (−0.012) indicating that the assumption made above regarding minimal carbonate production/dissolution, which is the only process unaccounted for and would act to shallow the observed slope, is a valid one. Our reported slope of −0.011 corresponds to a fractionation factor of −22.4‰ (Eq. 3), which is comparable to the chosen value used earlier in the analysis (−25‰) and provides a baseline estimate for comparison in future studies.

The use of DIC_{bio} successfully disentangles the various processes shown in Fig. 5a and provides further evidence that the production and respiration of organic matter by biological processes largely governs the relationship between DIC and its isotopic composition in the North Sea. Furthermore, this computed slope now quantifies the relationship between $\delta^{13}C_{DIC}$ and the biological uptake/production of DIC: a $\delta^{13}C_{DIC}$ signature change of −0.011‰, relates to a release of 1 $\mu mol/kg$ DIC. This slope can be used to relate $\delta^{13}C_{DIC}$ values to biological changes in DIC concentrations. This theoretical "metabolic DIC" (DIC_{meta}) differs from DIC_{bio} as it is computed using $\delta^{13}C_{DIC}$ and the slope from Fig. 5b. Nevertheless, DIC_{meta} is derived from DIC_{bio}, and thus is also considered a relative variable, meaning only relative changes in DIC_{meta} will be considered here.

Tracing metabolic DIC sources using radium

As discussed above, the relative balance between production and respiration governs the $\delta^{13}C_{DIC}$ signature throughout the majority of North Sea surface waters. In stratified water columns, a separation is caused by vertical transport (sinking) of organic material out of surface waters. The extent of this separation, and thus the $\delta^{13}C_{DIC}$ signatures in the surface waters of the stratified northern region, could vary spatially due to differences in productivity or mixed layer depth. Yet, considerable variability in $\delta^{13}C_{DIC}$ is observed throughout the entire North Sea, in particular within the fully mixed southern region (Fig. 2a), where

pelagic production and respiration should be relatively well-balanced. In fact, within the southern North Sea, a nearshore to offshore gradient is visible in the surface distributions of $\delta^{13}C_{DIC}$ (Fig. 2a), with surface waters becoming isotopically heavier with increased distance from the continental coastline. Given the well-mixed nature of $\delta^{13}C_{DIC}$ profiles in the southern North Sea (Fig. 3), variability in surface waters requires the presence of a non-pelagic carbon source with a different carbon isotopic signature.

One such source could be the underlying sediment. Respiration of organic matter creates a buildup of isotopically depleted DIC within sediment pore waters, which is eventually released during sediment-water column interaction. If, for example, production and respiration in the fully mixed water column are decoupled by prolonged deposition of organic matter on the seafloor, the sediments could represent a spatially varying carbon source with a net respiratory $\delta^{13}C_{DIC}$ signal. In the southern North Sea, a spring to summer transition between CO_2 undersaturation and supersaturation has been linked to the decoupling of production during the spring bloom, and respiration of that organic material later in the summer (Thomas et al. 2004). Delayed remineralization of the organic matter formed during the spring bloom was also observed by the North Sea coupled sediment-water model ECOHAM (Luff and Moll 2004).

A further, allochthonous source of carbon to the southern North Sea is the European coastline, where high DIC and AT, as well as low $\delta^{13}C_{DIC}$ are clearly visible (Figs. 2, 4). Winde et al. (2014a) observed an export of DIC from the Wadden Sea into the North Sea with a $\delta^{13}C_{DIC}$ of ∼-2.2‰, whereas Schwichtenberg (2013) concluded that exports from the Wadden Sea and Rhine Estuary (which comprise most of the North Sea European continental coastline) have significant impacts on DIC and AT concentrations throughout the North Sea. Lateral input of isotopically light carbon would create a net respiratory signal in surface water $\delta^{13}C_{DIC}$, and the dispersion of this signal throughout the southern North Sea would setup a nearshore to offshore gradient in $\delta^{13}C_{DIC}$ similar to the one shown in Fig. 2a. To help characterize the external carbon as either benthic or coastally sourced, we use ^{224}Ra and ^{228}Ra isotopes, which are considered to be strong tracers of sediment-water column and land-ocean interaction, respectively.

Figure 6 (panels a and c) show the relationships between $\delta^{13}C_{DIC}$ and both ^{224}Ra and ^{228}Ra isotopes. In general, both isotopes show a correlation with $\delta^{13}C_{DIC}$, with a visibly stronger correlation for ^{228}Ra. This figure illustrates that a higher Ra activity corresponds to a more depleted $\delta^{13}C_{DIC}$ signature, and thus an increase in the net respiratory signal. However, at low salinity stations this relationship is likely overlain by the characteristically high-Ra, low-$\delta^{13}C_{DIC}$ freshwater inputs. Similarly, points with very depleted Ra and enriched $\delta^{13}C_{DIC}$ correspond to surface waters at stations in the stratified northern region. At fully mixed stations with no discernable freshwater

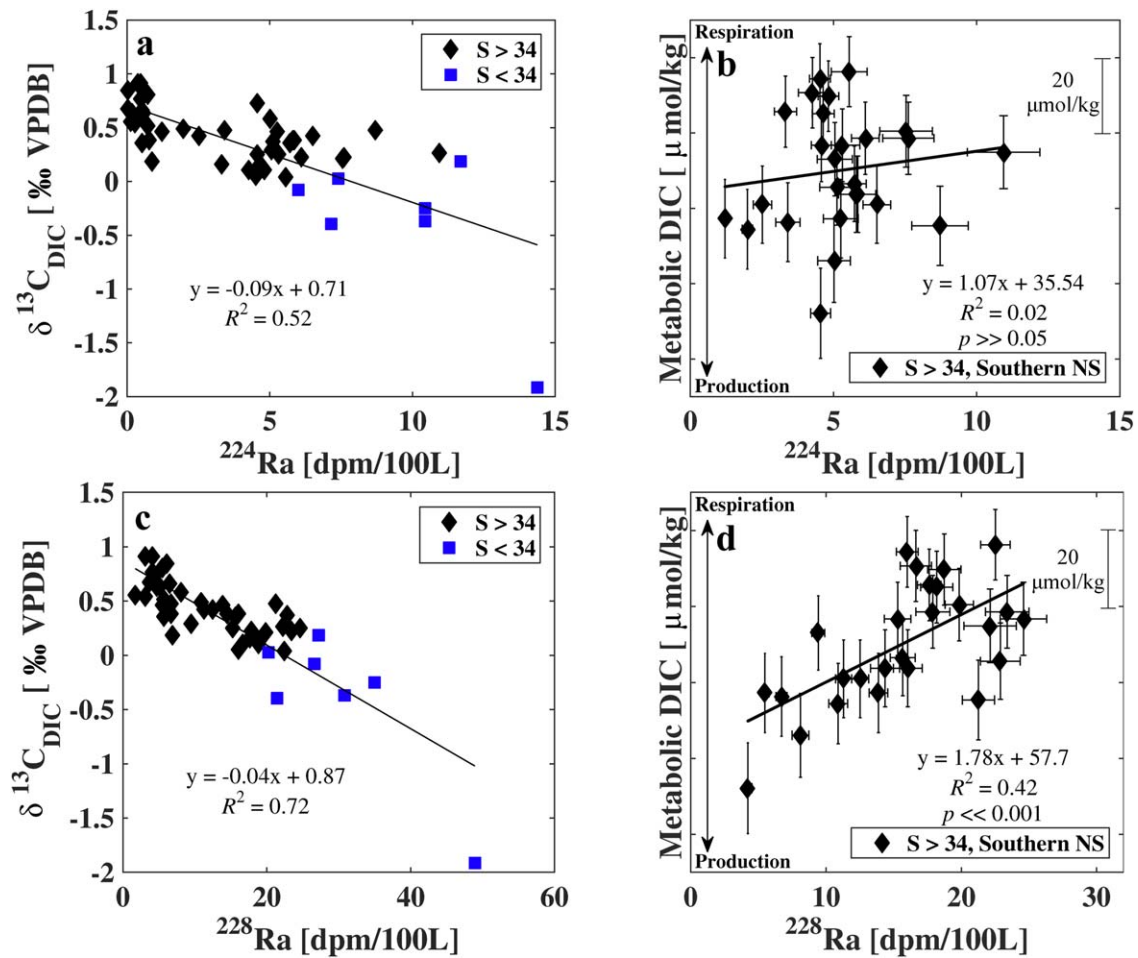**Fig. 6.** Left: Correlations between $\delta^{13}C_{DIC}$ and the ^{224}Ra (**a**) and ^{228}Ra (**c**) isotopes. Right: Correlations between Metabolic DIC and the ^{224}Ra (**b**) and ^{228}Ra (**d**) isotopes in well-mixed stations at salinities above 34. The *y*-axes contain no absolute values because metabolic DIC is a relative variable, but each tick mark represents a 20 μmol/kg change. Higher metabolic DIC is indicative of more organic matter respiration whereas lower values point to more production. Equations show the quality of the least-squares regressions, with the significance of the fit given by the *p*-values.

input, variability in $\delta^{13}C_{DIC}$ which is captured by differences in Ra activities can be attributed specifically to a benthic or coastal source of respiratory carbon.

To investigate this further, $\delta^{13}C_{DIC}$ values are converted into metabolic DIC concentrations and plotted against ^{224}Ra and ^{228}Ra at all fully mixed, southern North Sea stations without a discernible freshwater input (i.e., $S > 34$; Fig. 6b,d). In these panels, absolute values are not assigned to the *y*-axis, but each tick mark represents a change in metabolic DIC of 20 μmol/kg. A least-squares regression yields a slope that infers and quantifies the amount of metabolic DIC added for every measured unit of Ra.

No correlation is found between ^{224}Ra and metabolic DIC, indicating that a respiratory DIC source from sediments, if present, cannot be detected during the 1–2 week lifetime of the ^{224}Ra isotope (*see* also Burt et al. 2014). In contrast, a significant correlation exists between ^{228}Ra and metabolic DIC. Assuming ^{228}Ra is predominantly sourced

from the coastline, the strong correlation and the slope shown in Fig. 6d allows a coastally sourced metabolic DIC concentration to be inferred directly using ^{228}Ra activity.

^{228}Ra as a tracer of AT

The cycling of AT through the North Sea has been the subject of numerous studies (Kempe and Pegler 1991; Thomas et al. 2009). One common convention to identify important water masses influencing the carbonate system is to plot DIC or AT against salinity. In the North Sea, this leads to the identification of three main water masses: the central North Sea (or North Atlantic input), the Skagerrak (or Baltic Sea input), and the Southern (or German) Bight (Kempe and Pegler 1991; Bozec et al. 2005; Clargo et al. 2015). The relative abundances of these three water masses have been shown to significantly alter the pCO$_2$ and pH dynamics of the North Sea (Salt et al. 2013). Here, salinity plotted against AT (Fig. 7a) shows the same distinctions as in

these prior studies, with lower salinity waters from the Baltic (via the Skagerrak) and the European coastline (i.e., German Bight) influencing the AT throughout the North Sea. However, the North Atlantic endmember is not distinguishable from North Sea waters because salinity differences between the North Atlantic and central North Sea are too small. In contrast, typical ^{228}Ra activities in the open North Atlantic are between 1 and 3 dpm/100 L (Kaufman et al. 1973), which is distinctly lower than the vast majority of the observed North Sea samples. As a result, plotting ^{228}Ra against AT (Fig. 7b) provides three distinct endmembers, all of which converge in the central North Sea.

The ^{228}Ra vs. AT plot (Fig. 7b) reveals features of the general circulation in the North Sea, and shows that characteristics of the surface AT distribution (Fig. 2f) can be more readily explained using ^{228}Ra compared to the conventional salinity relationship (shown in Fig. 7a). The low-^{228}Ra, high-AT stations are located in the northwest corner of the North Sea, and are indicative of offshore waters flowing in through the Shetland or Faire Island Channels. The high-^{228}Ra, high-AT stations are all bordering the European coastline, clearly indicating this region as a ^{228}Ra and AT source. Finally, Baltic water outflow, characterized by low-AT and intermediate ^{228}Ra, intrudes across the central North Sea creating the band of lower-AT waters between 53 and 56 degrees North (*see* Fig. 2).

Looking again at stations within the fully mixed southern North Sea, a relationship between ^{228}Ra and AT is found which is similar to that observed between ^{228}Ra and metabolic DIC (Fig. 6d). That is, in waters without a discernable freshwater input, increased AT is associated with increased ^{228}Ra, and the European coastline is an evident AT source. A least-squares regression through these points yields a slope of 1.80 μmol/kg increase in AT per unit of ^{228}Ra. Analogous to the result in the previous section, this slope can be used to calculate coastal AT inputs to the North Sea.

Coastal inputs of ^{228}Ra, DIC, AT

^{228}Ra activities can be presented as mixed layer inventories by integrating ^{228}Ra activities over the mixed layer depth, or for stations in the fully mixed southern North Sea, the water depth. Given the spatial coverage of the radium measurements (Fig. 2), these inventories provide a basin-wide estimate of coastal ^{228}Ra inputs, or in other words, the total terrestrial ^{228}Ra input to the North Sea. First, to exclusively attribute the ^{228}Ra inventories to the European continental coastline, activities are expressed as excess ^{228}Ra, or the activity in excess of the background activity in North Atlantic waters. Here, the background value of 1.75 dpm/100L is chosen based on our lowest measured activity, which is located at the highest salinity station (station 48, 57.0°N, 0.9°E) in the northwestern North Sea where North Atlantic waters presumably enter (*see* Fig. 2). An area-weighted linear interpolation across the sampling grid yields an average inventory across the entire basin, which, multiplied by the surface area of the domain, yields a total inventory of 9.3×10^{14} dpm. Both the observed and interpolated inventory data are shown in Fig. 8a. Dividing this basin-wide inventory by an approximated length of the European continental coastline (620 km) yields an inventory of 1.5×10^{12} dpm per km of coastline, which compares well to the inventories reported by Moore (2007) for the Southeastern Bight ($0.7\text{-}1.3 \times 10^{11}$ dpm per km of coastline).

The slopes (*M*) displayed in Figs. 6d, 7b can be used to infer metabolic DIC and AT concentrations using the ^{228}Ra activity at a given station. Consequently, inventories (*I*) of metabolic DIC or AT per unit area of water column can be calculated using the depth (*z*) and density (ρ) at a given station:

$$I[\mu\text{mol C/m}^2] = (ex^{228}Ra * M)\,[\mu\text{mol/kg}] * \rho[\text{kg/m}^3] * z[\text{m}] \quad (4)$$

The ex^{228}Ra term refers to the excess ^{228}Ra activity. The spatial distribution of metabolic DIC inputs throughout the southern North Sea is shown in Fig. 8b. The distribution of metabolic AT inputs looks very similar to that of metabolic
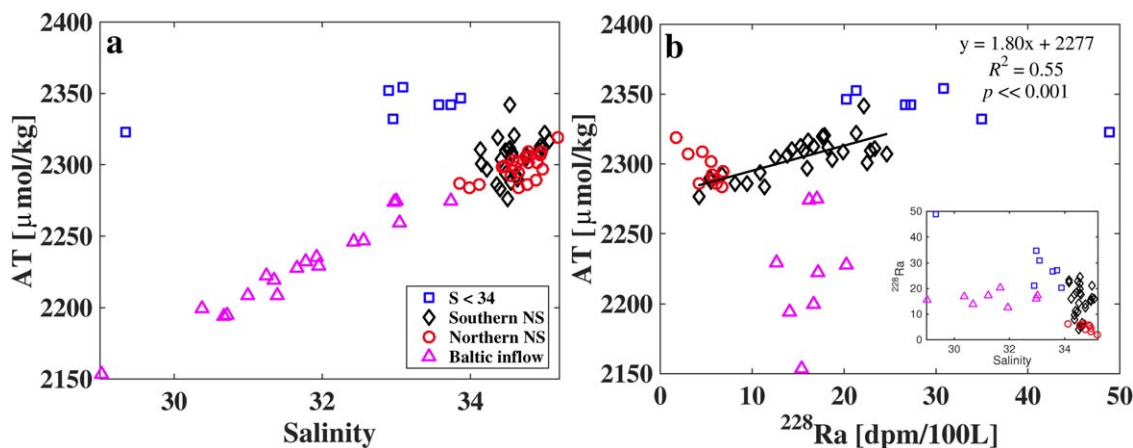

Fig. 7. Comparison of water mass distinctions using **(a)** Salinity against AT and **(b)** ^{228}Ra against AT. Inset diagram (salinity against ^{228}Ra) shows that southern NS stations (black diamonds) have no salinity dependence. The legend shown in the left panel applies to all plots.
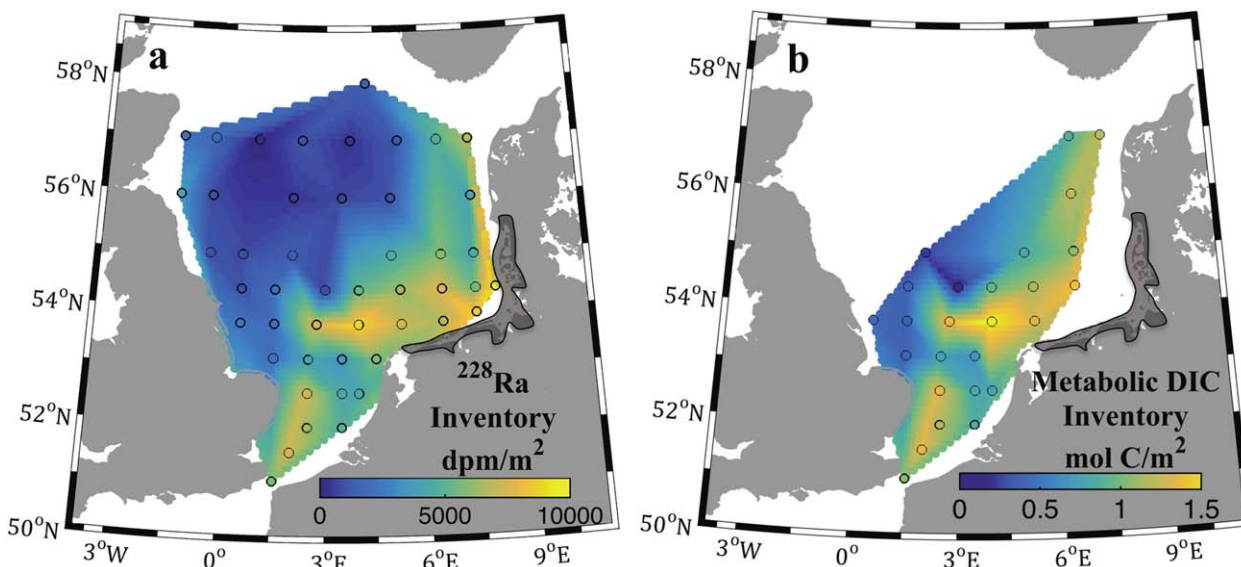
Fig. 8. a: Basin-wide **(a)** ^{228}Ra and **(b)** metabolic DIC inventories. ^{228}Ra inventories are calculated at all stations excluding the Skagerrak, whereas DIC inventories are limited to southern North Sea stations where the relationship between $\delta^{13}C_{DIC}$ and DIC$_{bio}$ is applied. Filled black circles represent discrete inventory values at the station locations and values in between are calculated using the area-weighed linear interpolation scheme. The area of the colored domain represents the surface area used in the calculations. Area outlined in black represents the Wadden Sea.

DIC because the two slopes used are nearly identical. The distribution of metabolic DIC further suggests that the primary source of metabolic DIC and AT is the coastline, and more specifically, the Wadden Sea (*see* Fig. 8b). Larger inventories are also observed near the English Channel or the southern UK coast. Metabolic DIC inventories at individual stations range from 0.14 ± 0.06 to 1.62 ± 0.44 mol C/m^2. These water-column inputs correspond to alterations in surface DIC concentrations of 4–41 μmol/kg. For comparison, mean surface DIC concentrations in the German Bight exhibit seasonal variations of $\sim$ 40–70 μmol/kg (Bozec et al. 2006; Schwichtenberg 2013). Metabolic AT inventories ranged from 0.15 ± 0.05 to 1.64 ± 0.34 mol AT/m^2, corresponding to alterations in surface water AT concentrations (4–41 μmol/kg) that are also similar in magnitude to seasonal variations in the North Sea ($\sim$ 17–33 μmol/kg) (Schwichtenberg 2013). In a recent modeling study, Schwichtenberg (2013) investigated the effect of Wadden Sea AT export by comparing simulated German Bight AT concentrations with and without additions from the Wadden Sea. The results showed that the average September AT concentrations in the German Bight increase by 18–30 μmol/kg when Wadden Sea exports are included. These values are almost identical to the coastal AT inputs calculated here, which we assume to come mostly from the Wadden Sea.

Basin-wide additions of metabolic DIC and AT to the southern North Sea are estimated at 1.20×10^{11} mol C and 1.21×10^{11} mol AT respectively. Using a 90-d residence time for southern North Sea waters (Lenhart and Pohlmann 1997) the metabolic DIC inventory equates to a terrestrial metabolic DIC flux of approximately 4.87×10^{11} mol C/year,

which is comparable to the riverine DIC flux to the entire North Sea (7.78×10^{11} mol C/year, Thomas et al. 2005). Although these basin-wide calculations represent first-order estimates, it can be generally concluded that the European continental coastline is a substantial source of metabolic DIC and AT that can impact the overall biogeochemistry of the North Sea.

Metabolic pathways of DIC and AT production

According to the results above, coastal input provides nearly equal amounts of biologically produced DIC and AT. If metabolic DIC was predominantly produced by aerobic respiration, it is expected that this input would exhibit net AT consumption, with an approximate DIC/AT ratio of -6.6. Here, the calculated DIC/AT ratio of $+0.99$ is indicative of a substantial contribution from anaerobic processes, and more specifically, denitrification, which produces near-equal amounts of DIC and AT (DIC/AT = 1.25). Other anaerobic processes (e.g., sulphate reduction, DIC/AT = 0.5), combined with aerobic respiration could produce a similar ratio. However, the reduction of iron, manganese, and sulphate, all of which produce more AT than DIC, are fully reversible reactions (assuming negligible pyrite burial) wherein the AT produced under anoxic conditions will be consumed in the oxygenated sediment or water column via reoxidation of the reduced compounds (Fe^{2+}, Mn^{2+}, and H_2S). Therefore, the presence of this substantial metabolic AT signal in the oxygenated waters of the southern North Sea suggests the dominance of denitrification, which irreversibly produces N_2. Furthermore, the metabolic AT input represents a net AT addition, which can only be produced by the denitrification
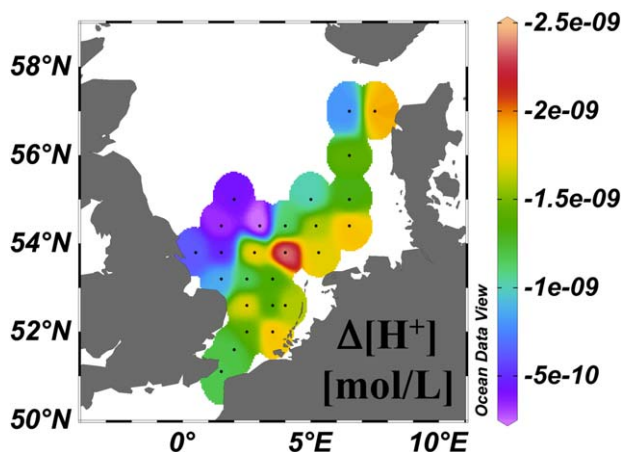
Fig. 9. Changes in proton concentration ($\Delta[H^+]$) induced by removing the coastal AT input from the observed AT, recalculating [H^+], and comparing this value to the observed [H^+]. For reference, the largest value, located at station 16 (53.8°N, 4.8°E, red color), is equivalent to a drop in pH from 7.99 to 7.90 at that station, while the difference at the furthest offshore station (55.0°N, 2.0°E, purple color), corresponds to a drop in pH from 8.07 to 8.06.

of allochthonous nitrate (e.g., terrestrial nitrate from rivers or groundwater).

Denitrification of land-derived nitrate as the dominant mechanism producing the observed metabolic inputs provides further evidence of a predominantly coastal source from the European coastline rather than a benthic source from the southern North Sea. Although denitrification can occur in the permeable sands of the open North Sea and the Wadden Sea (Gao et al. 2010), benthic fluxes for southern North Sea stations measured by Brenner et al. (2015) during the 2011 cruise exhibit DIC/AT ratios that are generally greater than 1.25, which likely reflects the greater importance of aerobic respiration. In the shallow tidal sediments of the Wadden Sea, anaerobic processes are dominant (Böttcher et al. 1998, 2000; Kowalski et al. 2012), resulting in lower DIC/AT ratios (Schwichtenberg 2013). Furthermore, denitrification rates in the Wadden Sea are among the highest observed for any marine environment (Gao et al. 2010), suggesting that this region is capable of producing the metabolic inputs observed in this study.

Coastal inputs as a buffer against acidification

The calculated export of metabolic AT from the European continental coastline affects the acid–base buffering capacity of the southern North Sea. To further investigate this, the potential change in proton concentration ([H^+]) induced by removing the coastally sourced AT from the observed values, is quantified (Fig. 9). Under the observed conditions, this corresponds to a surface pH decrease at southern North Sea stations between 0.01 and 0.09 units. According to Provoost et al. (2010), the past 2 decades have seen annual pH declines of a similar magnitude in the southern North Sea

(-0.02 to -0.03 pH units per year). This represents an order of magnitude faster rate of ocean acidification compared with the open North Atlantic (-0.0017 pH units per year) (Santana-Casiano et al. 2007).

In the southern North Sea, pH has followed an increasing trend throughout the 1970s and early 1980s, mirroring the same trend in riverine nitrate loadings (Pätsch and Lenhart 2011) (Fig. 10a). In contrast, a reversal of these trends has been observed from the late 1990s onward (Provoost et al. 2010) with strongly declining levels of both pH and nitrate runoff (Fig. 10b). It is thought that increases in the nutrient delivery enhanced primary productivity, and that declines in primary productivity in recent decades can be attributed to a decrease in riverine nutrient delivery. The concomitant increase or decrease in pH then resulted from increased or declining biological CO_2 uptake, respectively (Borges and Gypens 2010; Provoost et al. 2010). However, at the annual timescale, DIC will re-equilibrate with atmospheric CO_2 in the well-ventilated waters of the southern North Sea, causing biologically driven changes in the standing stock of DIC to largely vanish. The surface water pCO_2 and pH should adopt the atmospheric secular trend of rising CO_2 conditions, i.e., should broadly reflect the trend of ocean acidification (OA) as observed in the open oceans. However, as shown in Fig. 10, the observed trends in pH oppose the open ocean OA trend with rising pH in the late 70s to mid-80s. On the contrary the open ocean OA trend appears amplified by an order of magnitude during the more recent years.

Here, we suggest a complementary mechanism for the observed pH trends that refers back to changes in alkalinity, and would act synergistically with productivity-driven changes in DIC. During the observed pH increase, the North Sea was subject to intense coastal eutrophication, fueled primarily by riverine nitrate (and general nutrient loading; Fig. 10a) (Pätsch and Radach 1997; Gypens et al. 2009). Upon depletion of the oxygen reservoir in the upper sediment, the denitrification of the land-derived (i.e., allochthonous) nitrate releases (respiratory) AT, and the extent of denitrification is assumed to scale with the allochtonous nitrate loading (van Beusekom and de Jonge 2002; Vichi et al. 2004). The denitrification of the allochthonous nitrate thus creates an increase in the standing stock of AT, raising the pH and buffering or even overruling the pH decline driven by ocean acidification (Fig. 10a). Since the early 1990s measures to reduce nutrient runoff from the European continent have caused a decline in coastal eutrophication, paralleled by decreases in primary productivity (Borges and Gypens 2010). A reduction in denitrification leads to a diminished release of respiratory AT, which will cause the water column's equilibration with atmospheric CO_2 to result in a stronger decline in pH than under "high AT" conditions, thus amplifying the impacts of ocean acidification. Therefore, we argue that the respiratory AT release into the coastal waters reported here is substantially smaller currently than in previous decades,
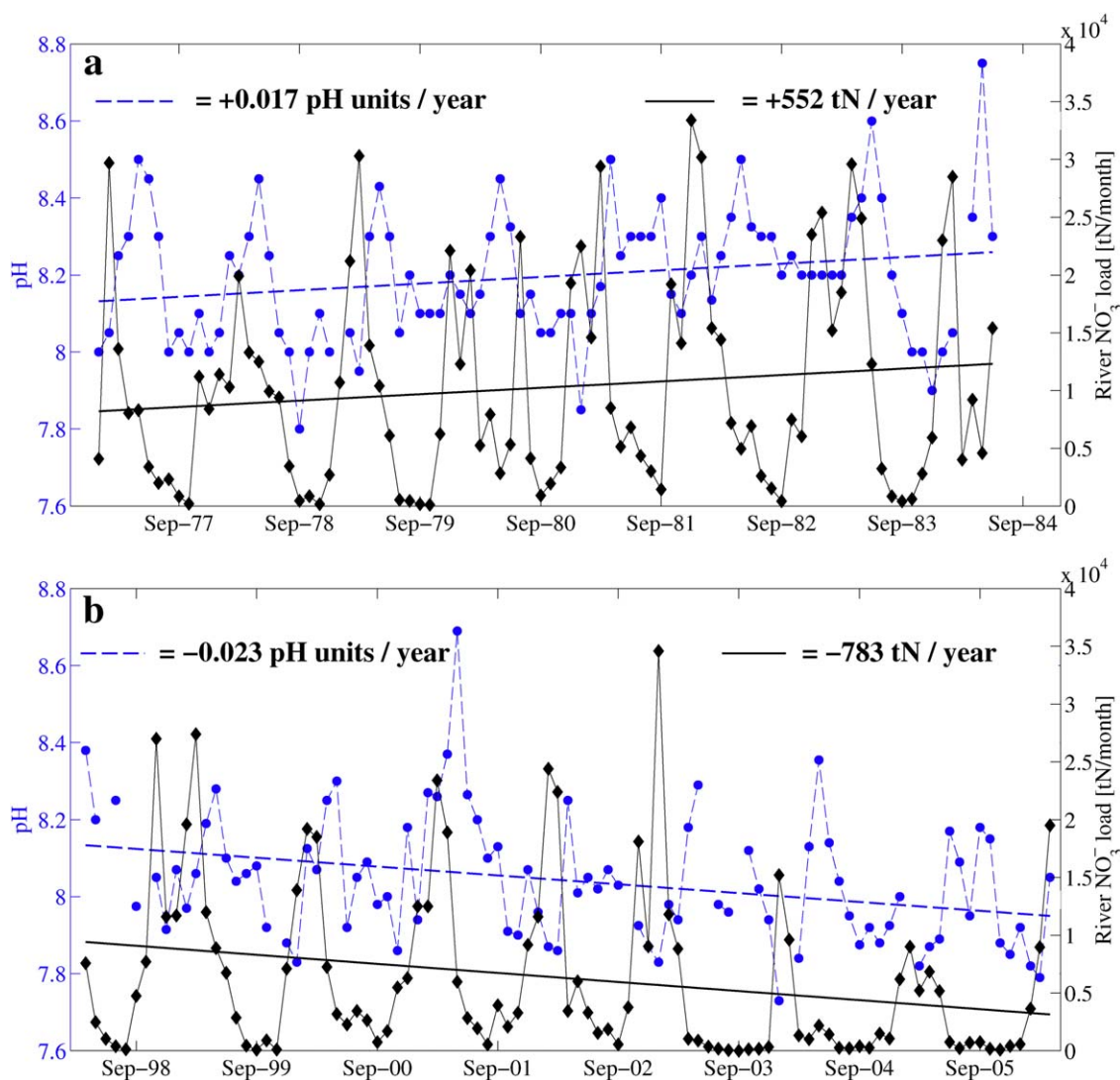
Fig. 10. Monthly time-series of pH (blue circles) and riverine nitrate (NO_3^-) loads (black diamonds) from 1977–1984 (**a**) and 1998–2005 (**b**). Riverine nitrate is measured from Haringvliet (mouth of the Rhine and Maas rivers) and pH is measured 20 km offshore of Haringvliet, in the Dutch coastal zone. pH data extracted from Fig. 5 in Provoost et al. (2010), and NO_3^- data provided by Pätsch and Lenhart (2011).

which is reflected in observations of rapid pH decline since the 1990s (Provoost et al. 2010).

Figure 10 confirms that the pH trends in the Dutch coastal zone shown by Provoost et al. (2010) mimic very closely the trends in nitrate loads from the nearby Rhine and Maas rivers. The general seasonal pattern is maximum nitrate delivery in February/March, with the highest pH levels occurring 3 months later in May/June. Both signals decrease rapidly throughout the summer, with minimum runoff and pH occurring around September and December respectively. These larger, seasonal changes in pH can be attributed mostly to primary productivity, as the riverine nitrate is utilized rapidly during the spring bloom, and both organic matter remineralization and atmospheric CO_2 equilibration lead to pH decline through the summer and fall.

The multiyear pH trend, however, may be more related to changes in AT. More specifically, long-term trends in nitrate delivery alter the standing stock of AT, which regulates the pH during the stable fall and winter months, and, as described above, can amplify or even override the long-term effect of ocean acidification.

Overall, this is an indication that pH in the southern North Sea is closely linked to coastal AT generation fueled by denitrification of riverine nitrate, highlighting the importance of these coastal alkalinity inputs in regulating the pH balance of the North Sea. Also, these results demonstrate the clear need to monitor changes in biogeochemical cycling within coastal systems. Finally, given its effectiveness as a tracer of AT, these findings suggest that ^{228}Ra sampling should be considered during future North Sea observational

campaigns. Since water and element fluxes at the land-ocean interface will differ for the tidal basins, detailed inventories are required to quantify the importance of the different coastal regions on the North Sea carbonate system.

Summary and conclusions

This study furthers the understanding of the carbonate system in the North Sea in a variety of aspects. Surface distributions of ^{224}Ra, ^{228}Ra, and $\delta^{13}C_{DIC}$ indicate the importance of seafloor sediments and the European coastline as a source of these tracers, and show patterns relating to the presence, or absence, of stratification in the North Sea. The quantitative analysis of covariations between DIC and its isotopic signature ($\delta^{13}C_{DIC}$) and the use of DIC$_{bio}$ to disentangle the various processes causing covariation improves on the results of Winde et al. (2014a,b). Rate measurements for organic matter and carbonate production, as well as detailed analysis of the precise effect of anaerobic processes could improve this method further. Future studies could also expand on the basin-wide estimates of terrestrial ^{228}Ra and metabolic DIC and AT inputs that are made possible by high-resolution Ra sampling across the region. Finally, our results align with prior studies that have identified denitrification in the Wadden Sea as a potentially important mechanism for regulating acidification in the North Sea (e.g., van Beusekom et al. 2008) and augment this result with quantitative estimates of the coastal signal and its impact in the open North Sea.

References

Ahad, J. M., J. A. Barth, R. S. Ganeshram, R. G. Spencer, and G. Uher. 2008. Controls on carbon cycling in two contrasting temperate zone estuaries: The Tyne and Tweed, UK. Estuar. Coast. Shelf Sci. **78**: 685–693. doi:10.1016/j.ecss.2008.02.006

Amann, T., A. Weiss, and J. Hartmann. 2015. Inorganic Carbon Fluxes in the Inner Elbe Estuary, Germany. Estuaries Coasts **38**: 192–210. doi:10.1007/s12237-014-9785-6

Boehme, S., N. E. Blair, J. P. Chanton, and C. S. Martens. 1996. A mass balance of ^{13}C and ^{12}C in an organic-rich methane-producing marine sediment. Geochim. Cosmochim. Acta **60**: 3835–3848. doi:10.1016/0016-7037(96)00204-9

Borges, A., and N. Gypens. 2010. Carbonate chemistry in the coastal zone responds more strongly to eutrophication than to ocean acidification. Limnol. Oceanogr. **55**: 346–353. doi:10.4319/lo.2010.55.1.0346

Borges, A. V. 2011. Present day carbon dioxide fluxes in the coastal ocean and possible feedbacks under global change, p. 47–77. *In* P. Duarte and J. M. Santana-Casiano [eds.], Oceans and the atmospheric carbon content. Springer Science + Business Media B.V.

Böttcher, M. E. 1999. The stable isotopic geochemistry of the sulfur and carbon cycles in a modern karst environment. Isotopes Environ. Health Stud. **35**: 39–61. doi:10.1080/10256019908234078

Böttcher, M. E., B. Oelschläger, T. Höpner, H.-J. Brumsack, and J. Rullkötter. 1998. Sulfate reduction related to the early diagenetic degradation of organic matter and "black spot" formation in tidal sandflats of the German Wadden Sea (southern North Sea): Stable isotope (^{13}C, ^{34}S, ^{18}O) and other geochemical results. Org. Geochem. **29**: 1517–1530. doi:10.1016/S0146-6380(98)00124-7

Böttcher, M. E., and others. 2000. The biogeochemistry, stable isotope geochemistry, and microbial community structure of a temperate intertidal mudflat: An integrated study. Cont. Shelf Res. **20**: 1749–1769. doi:10.1016/S0278-4343(00)00046-7

Böttcher, M. E., A. M. Al-Raei, Y. Hilker, V. Heuer, K.-U. Hinrichs, and M. Segl. 2007. Methane and organic matter as sources for excess carbon dioxide in intertidal surface sands: Biogeochemical and stable isotope evidence. Geochim. Cosmochim. Acta **71**: A111. doi:10.1016/j.gca.2007.06.012

Bozec, Y., H. Thomas, K. Elkalay, and H. J. W. de Baar. 2005. The continental shelf pump for CO2 in the North Sea–evidence from summer observation. Mar. Chem. **93**: 131–147. doi:10.1016/j.marchem.2004.07.006

Bozec, Y., H. Thomas, L.-S. Schiettecatte, A. V. Borges, K. Elkalay, and H. J. W. de Baar. 2006. Assessment of the processes controlling seasonal variations of dissolved inorganic carbon in the North Sea. Limnol. Oceanogr. **51**: 2746–2762. doi:10.4319/lo.2006.51.6.2746

Brasse, S., A. Reimer, R. Seifert, and W. Michaelis. 1999. The influence of intertidal mudflats on the dissolved inorganic carbon and total alkalinity distribution in the German Bight, southeastern North Sea. J. Sea Res. **42**: 93–103. doi:10.1016/S1385-1101(99)00020-9

Brenner, H., U. Braeckman, M. Le Guitton, and F. J. R. Meysman. 2015. The impact of sedimentary alkalinity release on the water column CO$_2$ system in the North Sea. Biogeosci. Discuss. **12**: 12395–12453. doi:10.5194/bgd-12-12395-2015

Broecker, W. S., and E. Maier-Reimer. 1992. The influence of air and sea exchange on the carbon isotope distribution in the sea. Global Biogeochem. Cycles **6**: 315–320. doi:10.1029/92GB01672

Burt, W. J., H. Thomas, and J.-P. Auclair. 2013. Short-lived radium isotopes on the Scotian Shelf: Unique distributions and tracers of cross-shelf CO$_2$ and nutrient transport. Mar. Chem. **156**: 120–129. doi:10.1016/j.marchem.2013.05.007

Burt, W. J., and others. 2014. Radium isotopes as a tracer of sediment-water column exchange in the North Sea. Global Biogeochem. Cycles **28**: 786–804. doi:10.1002/2014GB004825

Charette, M. A. and J. C. Scholten. 2008. Marine Chemistry special issue: The renaissance of radium isotopic tracers in marine process studies. Mar. Chem. **109**: 185–187. doi:10.1016/j.marchem.2008.04.001

Clargo, N. M., L. A. Salt, H. Thomas, and H. J. W. de Baar. 2015. Rapid increase of observed DIC and pCO$_2$ in the surface waters of the North Sea in the 2001-2011 decade ascribed to climate change superimposed by biological processes. Mar. Chem. **177**: 566–581. doi:10.1016/j.marchem.2015.08.010

Deines, P., D. Langmuir, and R. S. Harmon. 1974. Stable carbon isotope ratios and the existence of a gas phase in the evolution of carbonate groundwaters. Geochim. Cosmochim. Acta **38**: 1147–1164. doi:10.1016/0016-7037(74)90010-6

Doney, S. C., V. J. Fabry, R. A. Feely, and J. A. Kleypas. 2009. Ocean acidification: The other CO2 problem. Ann. Rev. Mar. Sci. **1**: 169–192. doi:10.1146/annurev.marine.010908.163834

Dorsett, A., J. Chenier, J. B. Martin, and J. E. Cable. 2011. Assessing hydrological and biogeochemical controls on pore-water dissolved inorganic carbon cycling in a subterranean estuary: A ^{14}C and ^{13}C mass balance approach. Mar. Chem. **127**: 76–89. doi:10.1016/j.marchem.2011.07.007

Duarte, C. M., and others. 2013. Is ocean acidification an open-ocean syndrome? Understanding anthropogenic impacts on seawater pH. Estuaries Coasts **36**: 221–236. doi:10.1007/s12237-013-9594-3

Francey, R. J., C. E. Allison, D. M. Etheridge, and others. 1999. A 1000-year high precision record of δ^{13}C in atmospheric CO$_2$. Tellus. **51B**: 170–193.

Fry, B. 2002. Conservative mixing of stable isotopes across estuarine salinity gradients. A conceptual framework for monitoring watershed influences on downstream fisheries production. Estuaries **25**: 264–271. doi:10.1007/BF02691313

Gao, H., and others. 2010. Aerobic denitrification in permeable Wadden Sea sediments. ISME **4**: 417–426. doi:10.1038/ismej.2009.127

Garcia-Solsona, E., J. Garcia-Orellana, P. Masqu, and H. Dulaiova. 2008. Uncertainties associated with ^{223}Ra and ^{224}Ra measurements in water via a delayed coincidence counter (RaDeCC). Mar. Chem. **109**: 198–219. doi:10.1016/j.marchem.2007.11.006

Gruber, N., and others. 1999. Spatiotemporal patterns of carbon-13 in the global surface oceans and the oceanic Suess effect. Global Biogeochem. Cycles **13**: 307–335. doi:10.1029/1999GB900019

Gypens N., A. V. Borges, and C. Lancelot. 2009. Effect of eutrophication on air-sea CO$_2$ fluxes in the coastal Southern North Sea: A model study of the past 50 years. Global Change Biol. **15**: 1040–1056. doi:10.1111/j.1365-2486.2008.01773.x

Heuer, V. B., J. W. Pohlman, M. E. Torres, M. Elvert, and K.-U. Hinrichs. 2009. The stable carbon isotope biogeochemistry of acetate and other dissolved carbon species in deep sub seafloor sediments at the northern Cascadia Margin. Geochim. Cosmochim. Acta **73**: 3323–3336.doi:10.1016/j.gca.2009.03.001

Hoefs, J. 2015. Stable isotope geochemistry, 7th ed. Springer Science.

Hu, X., and D. Burdige. 2007. Enriched stable carbon isotopes in the pore waters of carbonate sediments dominated by seagrasses: Evidence for coupled carbonate dissolution and reprecipitation. Geochim. Cosmochim. Acta **71**: 129–144. doi:10.1016/j.gca.2006.08.043

Inoue, H., and Sugimura, Y. 1985. Carbon isotopic fractionation during the CO$_2$ exchange process between air and sea water under equilibrium and kinetic conditions. Geochim. Cosmochim. Acta **49**: 2453–2460. doi:10.1016/0016-7037(85)90245-5

Kaufman, A., R. Trier, W. Broecker, and H. Feely. 1973. Distribution of 228Ra in the world ocean. J. Geophys. Res. **78**: 8827–8848. doi:10.1029/JC078i036p08827

Kempe, S., and K. Pegler. 1991. Sinks and sources of CO2 in coastal seas: The North Sea. Tellus Ser. B **43**: 224–235. doi:10.1034/j.1600-0889.1991.00015.x

Kowalski, N., O. Dellwig, M. Beck, and others. 2012. A comparative study of manganese dynamics in the water column and sediments of intertidal systems of the North Sea. Est. Coast. Shelf Sci. **100**: 3–17. doi:10.1016/j.ecss.2011.03.011

Kühn, W., J. Pätsch, H. Thomas, A. V. Borges, L.-S. Schiettecatte, Y. Bozec, and A. Prowe. 2010. Nitrogen and carbon cycling in the North Sea and exchange with the North Atlantic–A model study, Part II: Carbon budget and fluxes. Cont. Shelf Res. **30**: 1701–1716. doi:10.1016/j.csr.2010.07.001

Lee, A. J. 1980. North Sea: Physical Oceanography, p. 467–493. *In* F. T. Banner, M. B. Collins, and K. S. Massie [eds.], The North-west European shelf Seas the seabed and the sea in motion II. Physical and Chemical Oceanography, Elsevier Oceanography Series, 24B, Elseveir.

Lenhart, H.-J., and T. Pohlmann. 1997. The ICES-boxes approach in relation to results of a North Sea circulation model. Tellus. **49A**: 139–160.

Lorkowski, I., J. Pätsch, A. Moll, and W. Kühn. 2012. Interannual variability of carbon fluxes in the North Sea from 1970 to 2006–Competing effects of abiotic and biotic drivers on the gas exchange of CO$_2$. Estuar. Coast. Shelf Sci. **100**: 38–57. doi:10.1016/j.ecss.2011.11.03

Luff, R., and A. Moll. 2004. Seasonal dynamics of the North Sea sediments using a three-dimensional coupled sediment–water model system. Cont. Shelf Res. **24**: 1099–1127.doi:10.1016/j.csr.2004.03.010

Lynch-Stieglitz, J., T. F. Stocker, W. S. Broecker, and R. G. Fairbanks. 1995. The influence of air-sea exchange on the isotopic composition of oceanic carbon: Observations and

modeling. Global Biogeochem. Cycles **9**: 653–665. doi: 10.1029/95GB02574

Michaelis, J., E. Usdowski, and G. Menschel. 1985. Partitioning of ^{13}C and ^{12}C on the degassing of CO_2 and the precipitation of calcite—Rayleigh-type fractionation and a kinetic model. Am. J. Sci. **285**: 318–327. doi:10.2475/ajs.285.4.318

Moore, W., and others. 2011. Radium-based pore water fluxes of silica, alkalinity, manganese, DOC, and uranium: A decade of studies in the German Wadden Sea. Geochim. Cosmochim. Acta **75**: 6535–6555. doi:10.1016/j.gca.2011.08.037

Moore, W. S. 2007. Seasonal distribution and flux of radium isotopes on the southeastern US continental shelf. J. Geophys. Res. **112**: C10013. doi:10.1029/2007JC004199

Olsen, A., and others. 2006. Magnitude and origin of the anthropogenic CO_2 increase and ^{13}C Suess effect in the Nordic seas since 1981. Global Biogeochem. Cycles **20**: GB3027. doi:10.1029/2005GB002669

Olsen, A., and U. Ninnemann. 2010. Large 13C gradients in the preindustrial North Atlantic revealed. Science **330**: 658–659. doi:10.1126/science.1193769

Omar, A., A. Olsen, T. Johannessen, M. Hoppema, H. Thomas, and A. Borges. 2010. Spatiotemporal variations of fCO2 in the North Sea. Ocean Sci. **6**: 77–89. doi: 10.5194/os-6-77-2010

Orr, J. C., and others. 2005. Anthropogenic ocean acidification over the twenty-first century and its impact on calcifying organisms. Nature **437**: 681–686. doi:10.1038/nature04095

Pätsch, J., and G. Radach. 1997. Long-term simulation of the eutrophication of the North Sea: Temporal development of nutrients, chlorophyll and primary production in comparison to observations. J. Sea Res. **38**: 275–310. doi: 10.1016/S1385-1101(97)00051-8

Pätsch, J., and W. Kühn. 2008. Nitrogen and carbon cycling in the North Sea and exchange with the North Atlantica model study. Part I. nitrogen budget and fluxes. Cont. Shelf Res. **28**: 767–787. doi:10.1016/j.csr.2007.12.013

Pätsch, J., and H.-J. Lenhart. 2011. Daily loads of nutrients, total alkalinity, dissolved inorganic carbon and dissolved organic carbon of the European continental rivers for the years 1977-2009. Available from https://wiki.zmaw.de/ifm/ECOHAM/DATA_RIVER

Provoost, P., S. van Heuven, K. Soetaert, R. Laane, and J. Middelburg. 2010. Seasonal and long-term changes in pH in the Dutch coastal zone. Biogeosciences **7**: 3869–3878. doi:10.5194/bg-7-3869-2010

Prowe, A. F., and others. 2009. Mechanisms controlling the air–sea CO2 flux in the North Sea. Cont. Shelf Res. **29**: 1801–1808. doi:10.1016/j.csr.2009.06.003

Quay, P., and J. Stutsman. 2003. Surface layer carbon budget for the subtropical N. Pacific: ^{13}C constraints at station

Aloha. Deep-Sea Res.I **50**: 1045–1061. doi:10.1016/S0967-0637(03)00116-X

Quay, P., R. Sonnerup, J. Stutsman, J. Maurer, A. Körtzinger, X. Padin, and C. Robinson. 2007. Anthropogenic CO_2 accumulation rates in the North Atlantic Ocean from changes in the $^{13}C/^{12}C$ of dissolved inorganic carbon. Global Biogeochem. Cycles **21**: GB1009. doi:10.1029/2006GB002761

Racapé, V., and others. 2013. Anthropogenic carbon changes in the Irminger Basin (1981–2006): Coupling $^{13}CDIC$ and DIC observations. J. Mar. Sys. **126**: 24–32. doi:10.1016/j.jmarsys.2012.12.005

Salt, L. A., H. Thomas, A. Prowe, A. V. Borges, Y. Bozec, and H. J. W. de Baar. 2013. Variability of North Sea pH and CO2 in response to North Atlantic oscillation forcing. J. Geophys. Res. Biogeosci. **118**: 1584–1592. doi:10.1002/2013JG002306

Santana-Casiano, J. M., M. González-Dávila, M.-J. Rueda, O. Llinás, and E.-F. González-Dávila. 2007. The interannual variability of oceanic CO2 parameters in the northeast Atlantic subtropical gyre at the ESTOC site. Global Biogeochem. Cycles **21**: GB1015. doi:10.1029/2006GB002788

Santos I. R., Beck M., Brumsack H.-J., Maher D.T., Dittmar T., Waska H., and Schnetger B. 2015. Porewater exchange as a driver of carbon dynamics across a terrestrial-marine transect: Insights from coupled ^{222}Rn and pCO_2 observations in the German Wadden Sea. Mar. Chem. **171**: 10–20. doi:10.1016/j.marchem.2015.02.005

Schmidt, C., C. Hanfland, P. Regnier, P. Van Cappellen, M. Schlüter, U. Knauthe, I. Stimac, and W. Geibert. 2011. ^{228}Ra, ^{226}Ra, ^{224}Ra and ^{223}Ra in potential sources and sinks of land-derived material in the German Bight of the North Sea: implications for the use of radium as a tracer. Geo.-Mar. Lett. **31**: 259–269. doi:10.1007/s00367-011-0231-5

Schwichtenberg, F. 2013. Drivers of the carbonate system variability in the southern North Sea: River input, anaerobic alkalinity generation in the Wadden Sea and internal processes. Ph.D. thesis. Univ. of Hamburg.

Schwichtenberg, F., and others. 2012. Impact of internal and external alkalinity fluxes on the carbonate system of the larger German Bight, v. 14. EGU General Assembly Conference Abstracts, 11029.

Spiker, E. 1980. The behavior of C-14 and C-13 in estuarine water; effects of in situ CO_2 production and atmospheric change. Radiocarbon **22**: 647–654.

Thomas, H., Y. Bozec, K. Elkalay, and H. J. W. de Baar. 2004. Enhanced open ocean storage of CO2 from shelf sea pumping. Science **304**: 1005–1008. doi:10.1126/science.1095491

Thomas, H., and others. 2005. The carbon budget of the North Sea. Biogeosciences **2**: 87–96. doi:10.5194/bg-2-87-2005

Thomas, H., and others. 2007. Rapid decline of the CO2 buffering capacity in the North Sea and implications for the

North Atlantic ocean. Global Biogeochem. Cycles **21**: GB4001. doi:10.1029/2006GB002825

Thomas, H., and others. 2009. Enhanced ocean carbon storage from anaerobic alkalinity generation in coastal sediments. Biogeosciences **6**: 267–274. doi:10.5194/bg-6-267-2009

Turrell, W., E. Henderson, G. Slesser, R. Payne, and R. Adams. 1992. Seasonal changes in the circulation of the northern North Sea. Cont. Shelf Res. **12**: 257–286. doi:10.1016/0278-4343(92)90032-F

van Beusekom, J. E. E., and V. N. de Jonge. 2002. Long-term changes in Wadden Sea nutrient cycles: Importance of organic matter import from the North Sea. Hydrobiologia **475**: 185–194. doi:10.1023/A:1020361124656

van Beusekom, J. E. E., S. Weigelt-Krenz, and P. Martens. 2008. Long-term variability of winter nitrate concentrations in the Northern Wadden Sea driven by freshwater discharge, decreasing riverine loads and denitrification. Helgol. Mar. Res. **62**: 49–57. doi:10.1007/s10152-007-0092-5

Vichi, M., P. Ruardij, and J. W. Baretta. 2004. Link or sink: A modelling interpretation of the open Baltic biogeochemistry. Biogeosciences **1**:79–100. doi:10.5194/bg-1-79-2004

Winde, V. 2013. On the impact of benthic and pelagic processes on the carbonate system of the North Sea wadden Sea (in German). Ph.D. thesis. Univ. of Greifswald.

Winde, V., M. E. Böttcher, P. Escher, P. Böning, M. Beck, G. Liebezeit, and B. Schneider. 2014a. Tidal and spatial variations of DI^{13}C and aquatic chemistry in a temperate tidal basin during winter time. J. Mar. Sys. **129**: 396–404. doi:10.1016/j.jmarsys.2013.08.005

Winde, V., M. E. Böttcher, P. Escher, P. Böning, M. Beck, G. Liebezeit, and B. Schneider. 2014b. Corrigendum to: Tidal and spatial variations of DI^{13}C and aquatic chemistry in a temperate tidal basin during winter time. [J. Mar. Sys. 129: 396–404]. J. Mar. Sys. **139**: 509. doi:10.1016/j.jmarsys.2014.09.008

Winde V., P. Escher, B. Schneider, P. Böning, A. M. Al-Raei, G. Liebezeit, and M. E. Böttcher. 2014c. Carbon isotopes in DIC trace submarine groundwater discharge and advective pore water efflux in tidal areas of the southern North Sea. Proceeding 23rd SWIM conference, Husum, 42–45.

Wootton, J. T., and C. A. Pfister. 2012. Carbon system measurements and potential climatic drivers at a site of rapidly declining ocean pH. PLoS One **7**: e53396. doi:10.1371/journal.pone.0053396

Zeebe, R. E., and D. Wolf-Gladrow. 2001. CO2 in Seawater: Equilibrium, Kinetics, Isotopes. Elsevier Science.